JOURNAL OF PROPULSION AND POWER
Vol. 17, No. 2, March–April 2001

Mole-Fraction-Sensitive Imaging of Hypermixing Shear Layers

J. S. Fox,* A. F. P. Houwing,† and P. M. Danehy‡
Australian National University, Acton, Australian Capital Territory 0200, Australia
and
M. J. Gaston,§ N. R. Mudford,¶ and S. L. Gai**
University of New South Wales, Campbell, Australian Capital Territory 2612, Australia

A theoretical model that determines the optimum excitation frequency for obtaining a fluorescence signal with a strong dependence on fuel mole fraction is presented for supersonic fuel–air compressible mixing studies. The challenge associated with this is to maintain a high sensitivity to fuel mole fraction with minimal sensitivity to temperature and pressure in a flow with large temperature variations and pressure gradients. The results of the model are applied to the mixing region behind various scramjet fuel injectors in a shock tunnel to measure fuel mole fraction. Hydrogen fuel at a Mach number of 1.7 is injected into a mostly N_2 freestream at Mach 4.8. Experimental fluorescence images are presented in streamwise and spanwise planes.

Nomenclature

A	=	effective spontaneous emission rate, s^{-1}
A_{las}	=	cross-sectional area of the laser sheet, m^2
B	=	Einstein coefficient for absorption, $s^{-1} \cdot (J \cdot m^{-2} \cdot Hz^{-1})^{-1}$
C_{opt}	=	overall conversion efficiency, dimensionless
c_p	=	heat capacity at constant pressure, $J \cdot mol^{-1}k^{-1}$
$c_{p,fuel}$	=	heat capacity of pure fuel stream, $J \cdot mol^{-1}k^{-1}$
$c_{p,\infty}$	=	heat capacity of pure freestream, $J \cdot mol^{-1}k^{-1}$
E	=	energy of rotational state, J
E_p	=	laser energy per pulse, J
$f_{J''}$	=	Boltzmann fraction of the absorbing state
g	=	spectral overlap integral, $1/cm^{-1}$
g_a	=	absorption line shape, $1/cm^{-1}$
g_l	=	spectral profile of laser, $1/cm^{-1}$
J	=	rotational quantum number
J''	=	rotational quantum number of lower laser-coupled state
K	=	fluorescence signal per mole-fraction of fuel, counts
K_{max}	=	maximum fluorescence signal per mole-fraction of fuel, counts
k	=	Boltzmann's constant, $J \cdot kg^{-1}$
m_{NO}	=	molecular mass of NO, kg
m_p	=	molecular mass of perturbing species, kg
P	=	pressure, Pa
Q	=	total collisional quenching rate, s^{-1}
S	=	fluorescence signal, counts
S_{max}	=	maximum fluorescence signal, counts
T	=	temperature, K
T_{fuel}	=	temperature of pure fuel stream, K
T_{mix}	=	temperature of fuel–freestream gas mixture, K
T_∞	=	temperature of pure freestream, K
$\langle v_{NO} \rangle$	=	thermal velocity of NO, ms^{-1}
$\Delta\nu_a$	=	absorption linewidth in wave numbers, cm^{-1}
$\Delta\nu_l$	=	laser linewidth in wave numbers, cm^{-1}
δS_i	=	uncertainty in fluorescence signal due to $\delta\zeta_i$, counts
$\delta\zeta_i$	=	uncertainty in ith parameter
ϵ_i	=	sensitivity of fluorescence signal the ith parameter
ζ_i	=	ith generalized parameter
ν_a	=	absorption line frequency in wave numbers, cm^{-1}
ν_l	=	laser frequency in wave numbers, cm^{-1}
$\langle\langle\sigma\rangle\rangle$	=	total quenching cross section, m^2
$\langle\langle\sigma_p\rangle\rangle$	=	quenching cross-section of perturbing species, m^2
ϕ	=	fluorescence yield
χ_a	=	mole fraction of the absorbing species
χ_{fuel}	=	fuel mole fraction
χ_p	=	mole fraction of perturbing species

Subscripts

fuel	=	fuel
i	=	subscript for labeling generalized parameter
max	=	maximum value
NO	=	nitric oxide
p	=	perturbing species
∞	=	freestream

Superscript

$''$	=	lower laser-coupled state

Received 6 June 1999; revision received 14 August 2000; accepted for publication 14 August 2000.

*Graduate Student, Aerophysics and Laser-Based Diagnostics Research Laboratory, Department of Physics and Theoretical Physics.
†Associate Professor, Aerophysics and Laser-Based Diagnostics Research Laboratory, Department of Physics and Theoretical Physics. Member AIAA.
‡Lecturer, Aerophysics and Laser-Based Diagnostics Research Laboratory, Department of Physics and Theoretical Physics. Member AIAA.
§Graduate Student, University College, Department of Aerospace and Mechanical Engineering. Student Member AIAA.
¶Senior Lecturer, University College, Department of Aerospace and Mechanical Engineering. Member AIAA.
**Associate Professor, University College, Department of Aerospace and Mechanical Engineering. Associate Fellow AIAA.

Introduction

A PROPOSED propulsion system for the next generation of aerospace planes is the supersonic combustion ramjet (scramjet). It is perhaps the most promising candidate for an airbreathing engine capable of operating at hypersonic speeds. One of the challenges associated with the design of a successful prototype scramjet is the requirement to achieve a sufficiently high degree of mixing between the fuel and air so that the injected fuel undergoes combustion before its expulsion from the vehicle.

It is well known that mixing of air and fuel at supersonic speeds is not efficient.[1] Mixing enhancement is, therefore, necessary to ensure that combustion occurs sufficiently rapidly to provide adequate thrust. This can be assisted by fuel injector design. One method of mixing enhancement that is being investigated is termed hypermixing[2,3] with fuel injectors that employ this method being called hypermixers. Hypermixers generate streamwise vorticity that increases the surface contact between the fuel and air streams. The aim of this investigation is to qualitatively and quantitatively study

the performance of such hypermixing fuel injectors using an instantaneous, quantitative planar laser-induced fluorescence (PLIF) mole-fraction imaging technique.[4]

Many traditional line-of-sight techniques have been used to study scramjet fuel injectors including schlieren, shadowgraph,[5,6] and interferometry.[3,7] However, these methods are limited to measurement of integrated properties along the line of sight. By contrast, PLIF is suitable for both qualitative flow visualization and quantitative measurements of complex three-dimensional flowfields. This technique provides species and quantum-state specific information with very good spatial and temporal resolution.

PLIF involves illuminating the flow with a thin sheet of laser light tuned to excite electronic transitions in a chemical species in the flow. Here, the species is nitric oxide (NO), which is a minor component in the flow being studied. The fluorescence induced by this illumination is focused onto an intensified charge-coupled device (ICCD) camera to produce an image of the fluorescence in that region. With judicious choice of transition and subsequent image processing, the technique can yield measurements of temperature,[8] pressure,[9] velocity[10] or be used for species imaging.[11–14] In cases where only a single laser and a single detector is used, many of these techniques rely on averaging a number of images, or taking a ratio of averaged images. However, the present flow is highly turbulent and nonrepeatable in detail. Therefore, a method that will give instantaneous quantitative information on mole fraction in a single measurement is required.

The PLIF signal is a function of temperature, pressure, species concentrations, and a number of known experimental parameters.[15] To measure the fuel mole fraction directly, a strategy must be developed to minimize the temperature and pressure dependencies of the PLIF signal. This can be achieved by the choice of gases used in the freestream and fuel and by choosing a laser frequency and linewidth that simultaneously excites both low- and high-J transitions.

The work reported here centers around the attempt to visualize the fuel mole fraction in the presence of pressure gradients and large temperature variations. This method is demonstrated through the investigation of mixing layers behind hypermixing fuel injectors injecting fuel into a Mach 4.8 coflowing freestream, with a convective Mach number of 0.64.

PLIF Theory

Flourescence Signal

The PLIF signal level S (number of counts recorded on a pixel of a detector) is a function of temperature, pressure, mole fraction, and a number of other known experimental parameters. Provided the assumptions of linear fluorescence, weak excitation, negligible laser beam attenuation, and negligible radiation trapping are valid, the fluorescence signal level is given by[15]

$$S = \frac{E_p}{A_{\text{las}}}\frac{\chi_a P}{kT}\left(\sum_i [f_{J''}Bg]\right)\left(\frac{A}{A+Q}\right)C_{\text{opt}} \tag{1}$$

where the summation is over all transitions, A is the effective rate of spontaneous emission for all directly and indirectly populated states, Q is the total collisional quenching rate of the electronic excited state, and C_{opt} is the efficiency with which photons emitted from the gas are converted to photoelectrons in the ICCD camera. C_{opt} depends on the arrangement of the collection optics, spectral filtering, temporal gating, photocathode quantum efficiency, and intensifier gain. The term $A/(A+Q)$ is known as the fluorescence yield ϕ.

The PLIF signal, as defined in Eq. (1), has both explicit and implicit dependencies on temperature and pressure. Implicit temperature dependencies enter the signal equation through the Boltzmann fraction, the spectral overlap integral, and the quenching rate. Pressure dependence is implicit in the overlap integral and the quenching rate. These terms are discussed in detail.

The Boltzmann fraction $f_{J''}$ expresses the population of rotational levels and is a function of temperature. It is given by[16]

$$f_{J''} = (2J''+1)\exp(-E/kT) \tag{2}$$

where J'' is the rotational quantum number of the lower rotational level and E is its energy. The spectral overlap integral[17]

$$g = \int_0^\infty g_l(\nu_l, \Delta\nu_l)g_a(\nu_a, \Delta\nu_a)\,\mathrm{d}\nu \tag{3}$$

determines the overlap between the laser spectrum and a particular transition. The absorption line shape g_a is assumed to be a Voigt profile; The functions g_l and g_a are normalized so that their individual integrals over all frequencies are unity. Shifts and broadening of transitions due to pressure and temperature are taken into account in the integral of the absorption lineshape.[18]

The quenching rate depends on both pressure and temperature, as well as the species present in the flow,[15]

$$Q = \langle v_{\text{NO}}\rangle\langle\!\langle\sigma\rangle\!\rangle(P/kT) \tag{4}$$

where $\langle v_{\text{NO}}\rangle = \sqrt{(8kT/\pi m_{\text{NO}})}$, and the total electronic quenching cross section is given by

$$\langle\!\langle\sigma\rangle\!\rangle = \sum_p \chi_p\langle\!\langle\sigma_p\rangle\!\rangle\sqrt{1+\frac{m_{\text{NO}}}{m_p}} \tag{5}$$

The summation in Eq. (5) is over all perturbing species p; χ_p, m_p, and $\langle\!\langle\sigma_p\rangle\!\rangle$ are the mole fraction, molecular mass, and quenching cross section of the perturbing species, respectively.

An understanding of the implicit temperature and pressures dependencies described by Eqs. (2–5) is important in developing a technique that is capable of instantaneous mole-fraction imaging with minimal temperature and pressure sensitivities.

χ_{NO} Imaging

In many applications of PLIF, a laser frequency that excites an isolated transition is chosen, ensuring that neighboring transitions do not contribute to the PLIF signal. This simplifies quantitative analysis. However, to measure the mole fraction directly, a strategy must be devised to minimize the temperature and pressure dependence of the signal. For example, by exciting a particular transition with a weak temperature dependence, Clemens[19] achieved a fluorescence signal that was directly proportional to the mole fraction of NO. However, the temperature range of his work (140–270 K) was far smaller than that required in our fuel–air mixing studies (190–700 K). Furthermore, the conditions used in his work are different from the chemical environment produced in our facility. These restrictions have provided the current motivation to develop a technique suitable for a larger temperature range and the required chemical environment.

The aim of this work is to produce a fluorescence signal proportional to NO mole fraction alone. From Eq. (1) this can be satisfied if the term

$$K \equiv \frac{E_p}{A_{\text{las}}}\frac{P}{kT}\left(\sum_i [f_{J''}Bg]\right)\left(\frac{A}{A+Q}\right)C_{\text{opt}} \tag{6}$$

is constant, independent of temperature and pressure.

For the purposes of calculation, it is assumed that the only variation in temperature is that due to the isobaric mixing of cold fuel with hot freestream gases and that differential diffusion can be neglected. The temperature of the mixture is then calculated using an enthalpy balance[20]:

$$T_{\text{mix}} = \frac{[\chi_{\text{fuel}}T_{\text{fuel}} + (1-\chi_{\text{fuel}})(c_{p,\infty}/c_{p,\text{fuel}})T_\infty]}{[\chi_{\text{fuel}} + (1-\chi_{\text{fuel}})(c_{p,\infty}/c_{p,\text{fuel}})]} \tag{7}$$

The subscripts, fuel, ∞, and mix refer to the pure fuel stream, pure freestream, and a mixture of the two, respectively. The heat capacity is a function of temperature, but is assumed to be constant in the

determination of T_{mix}. This is not expected to result in significant errors for the temperature range considered.

There are a number of variables available to adjust to achieve a constant value of K: the operating conditions, the gas compositions, and the frequency and linewidth of the laser.

The flow conditions were chosen to achieve moderate total enthalpy and to be near hypersonic while staying within the operating envelope of the shock tunnel. The freestream must be predominantly N_2 and the fuel mostly H_2 so that mixing can be analyzed without the complication of combustion. A freestream Mach number of 4.8 was chosen for the purpose of studying mixing under hypersonic conditions for comparison with results obtained elsewhere under supersonic conditions. Combustion was inhibited by using a lower static temperature, a lower static pressure, and a mostly N_2 freestream. The operating conditions of the fuel injector were chosen so that the fuel-jet static pressure equaled that of the freestream gas in the test section.

The amount of NO in the freestream was determined by the maximum tolerable absorption and the required quench rate Q. Absorption was limited to be less than 2% cm^{-1} to obtain relatively uniform illumination. This gives an upper bound to the amount of NO that can be present in the test section. If the amount of the quenching species is chosen such that $Q \gg A$ [see Eqs. (4) and (6)], this ensures that the implicit pressure dependence in the quenching cancels out the explicit pressure dependence of the PLIF signal. A tradeoff must be made here, because a quenching rate that is too high will produce a signal that is low, whereas a quenching rate that is too low will cause the signal to have a large pressure dependence. The desired concentration of NO is produced by filling the shock tube with 98% N_2 and 2% O_2 by volume and allowing the shock heating in the tube to create NO by chemical reaction. Some NO reduction occurs in the expansion through the hypersonic nozzle.

It is also necessary to have the quench rate uniform throughout the flow. This means that the value of quenching is approximately the same for all values of T_{mix}, so that the lifetime of the fluorescence in all regions of the image is the same. To address this problem, a trace amount of CO_2, which is nontoxic and a strong quencher,[20] was added to the H_2. With CO_2 present in only trace amounts, the fluid mechanical behavior of the fuel is indistinguishable from that of H_2.

Line Selection

The choice of laser excitation frequency is also very important in ensuring that variations in K are minimized. The Boltzmann fraction $f_{J''}$, which appears in Eq. (6) for K, is very different for low- and high-J lines. Low-J transitions are more highly populated at low temperatures, whereas high-J lines are more highly populated at high temperatures. By choosing the laser frequency to excite both low- and high-J transitions, the effective Boltzmann fraction can be fairly insensitive to variations in T_{mix}. Thus, this will produce a value for K over a range of T_{mix} that exhibits lower variation than that produced by tuning to a single, isolated transition. Calculations were completed over the entire A–X (0, 0) NO spectrum to find transitions that minimized variations in K while maximizing the signal. The optimal laser frequency was 44282.38 cm^{-1}, centred on the $^pP_{11}(27)$ transition. Once the excitation frequency is chosen, the absorption must be calculated again to check that it is still $\leq$2% cm^{-1}. If this is the case, the only parameter left to adjust is the laser linewidth. These calculations were repeated for the laser linewidths available, and then we chose the linewidth that minimized the temperature sensitivity of the fluorescence signal.

Figure 1 shows the contributions to K, from all of the lines overlapped by the laser and the combined value of these, for increasing amounts of fuel. Though a number of absorption transitions contribute to the fluorescence signal, the dominant ones are the $^pP_{11}(27)$, $^qQ_{22}(24)$, and $^sR_{21}(8)$ transitions. These three transitions clearly show the effect of the Boltzmann fraction on the signal: the $^sR_{21}(8)$ has a high signal for low temperatures, whereas the $^pP_{11}(27)$ and $^qQ_{22}(24)$ transitions have a high signal for higher temperatures. When summed together these produce a reasonably constant K and thus a signal that is proportional to the mole fraction of NO to within ±6.4% over the specified temperature range.

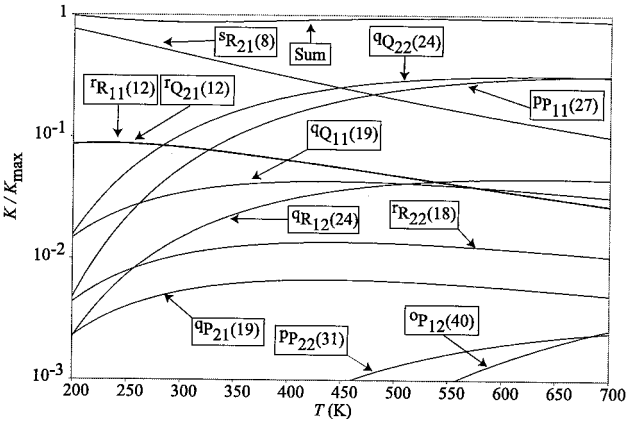

Fig. 1 Contribution of individual transitions to the total PLIF signal per mole of NO, K as defined by Eq. (6); K_{max} is the maximum total PLIF signal per mole of NO.

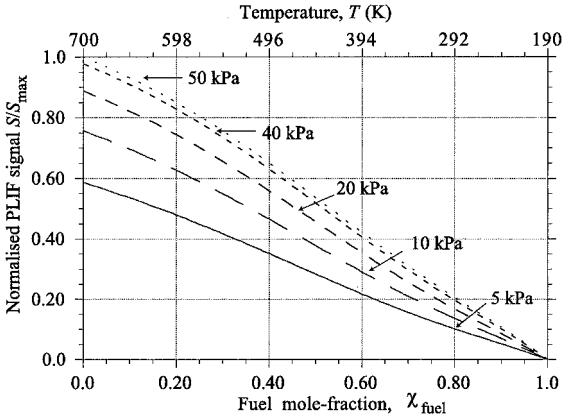

Fig. 2 PLIF signal level variation with pressures of 5, 10, 20, 40, and 50 kPa.

PLIF signal level variation for pressures of 5, 10, 20, 40, and 50 kPa is shown in Fig. 2. The PLIF signal S is normalized by the maximum signal S_{max} for the range under consideration. The signal decreases by about 40% in going from the 50-kPa case to the 5-kPa case, indicating that the PLIF signal is weakly dependent on pressure. To further reduce this pressure dependence, the quench rate could be increased, at the cost of reduced signal and/or increased absorption.

The PLIF signal is shown in Fig. 2 to be a monotonic function of fuel mole fraction at a given pressure. Therefore, the theoretical modeling can be used to convert experimental PLIF images to a quantitative measure of fuel mole fraction under constant pressure conditions, or in regions where the pressure has a known value.

Experiment

Flow Conditions and Model

The experiments were performed using a free-piston shock tunnel. A conical nozzle with a 125-mm-diam exit and 35-mm-diam throat was used to produce the required flow Mach numbers. Freestream conditions with a static pressure of 40 kPa, a static temperature of 700 K, and a Mach number of 4.8 were produced. The N_2/O_2 test gas mixture produced approximately 1.6% NO, 1.2% O_2, and 0.06% O, with a balance of N_2 by volume in the test section (calculated using the computer code STUBE[21]). The injected fuel was at a pressure of 40 kPa and a temperature of 190 K, giving a Mach number of 1.7. The fuel gas contained 0.3% CO_2 with a balance of hydrogen.

The supersonic flow produced by the tunnel passes over a centrally mounted plate into which each fuel injector is inserted. The fuel injectors used in this investigation are shown in Fig. 3. The view shown is that of the trailing edge of the injectors. For each injector,

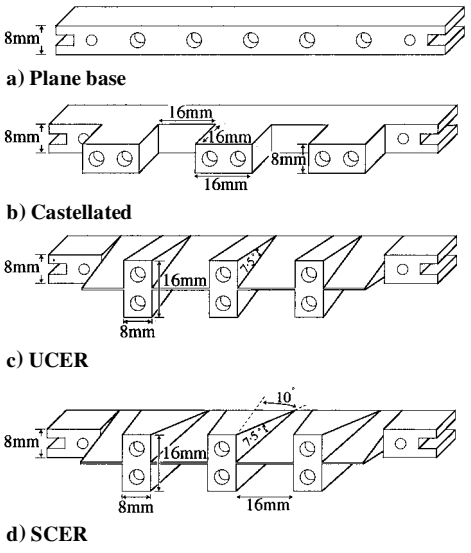

Fig. 3 Schematic of the fuel injectors used in the experiment. The view shown is that of the trailing edge of the injectors.

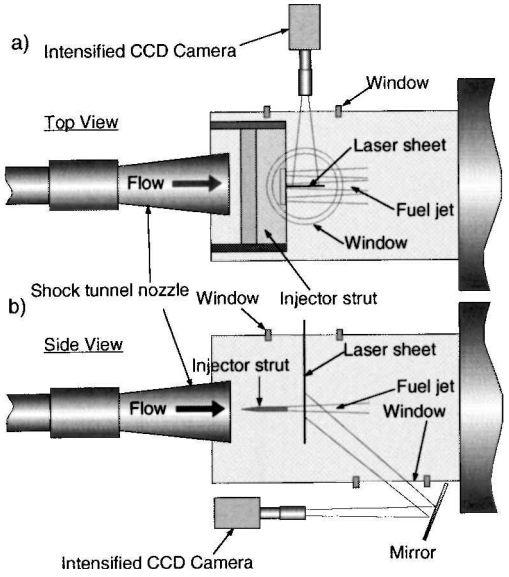

Fig. 4 Schematic of experimental setup for images: a) streamwise and b) spanwise.

each fuel nozzle has an exit diameter of 4.0 mm and a throat diameter of 3.5 mm. The thickness of the plate just upstream of the injector is taken to be the base height, 8 mm, for each injector. Figure 3a is the plane-base fuel injector and is used as the datum injector. The other three fuel injectors are hypermixers. Figure 3b is referred to as the castellated fuel injector because of its segmented blunt trailing edge.[22] Such trailing edges have been shown to reduce drag by converting some of the spanwise vorticity into streamwise vorticity.[3] Figure 3c is the unswept compression–expansion ramp (UCER) and Fig. 3d is the swept compression–expansion ramp (SCER) fuel injector, respectively.

For the castellated fuel injector, streamwise vorticity is generated by pressure differences between the projection surfaces and recess regions. In the case of the ramp fuel injectors, the pressure differences on the compression and expansion surfaces produce streamwise vorticity. The resultant streamwise vorticity forms into pairs of counter-rotating vortices that entrain the injected fuel. This causes the fuel–air interface to stretch and, therefore, increases the mixing. The addition of sweep to the compression–expansion ramp increases the strength of the vorticity generated.

A schematic of the experimental arrangement is shown in Fig. 4. The operation of the shock tunnel is described by Stalker.[23] Before

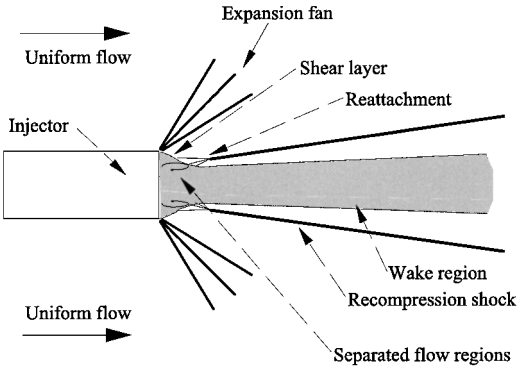

Fig. 5 Schematic of the flow over a scramjet injector; noninjection case.

firing the tunnel, the laser is tuned to a particular NO transition and pulsed at a fixed repetition rate. The recoil of the tunnel initiates an electronic trigger, which stops the laser from continuously triggering and, with a preset delay, triggers the injection system. A transducer in the nozzle reservoir region registers the shock reflection from the end of the shock tube, and the laser and camera systems are triggered 1.4 ms later. This delay corresponds to the time period during which the flow is steady in the test section.

Specific Flow Geometry

Figure 5 shows a schematic of the flow over a scramjet fuel injector, with a height of 8 mm, without fuel injection. The flow is uniform in the freestream and expands around the base of the fuel injector on both upper and lower surfaces. At the base of the fuel injector, a region of very hot, low-pressure separated flow forms. This low-speed recirculation region interacts with the high-speed inviscid region via the separated boundary layer that lies between them.

After its expansion around the base, a recompression shock forces the flow to move parallel to the freestream again. The flow between the recompression shocks is at approximately constant pressure because pressure can be considered to be approximately constant across a slowly growing shear layer. A wake region, having properties similar to the boundary layer at separation at the injector edge, is in the middle of the recompression shocks. The flow in the wake is hot and traveling slowly, whereas the flow between the wake and the recompression shocks is relatively cooler and faster. Therefore, the region between the recompression shocks has a uniform pressure but varying temperature, velocity, and density.

When fuel is injected, the flow is qualitatively similar, but the recompression shocks are further apart and the fuel jet issues into the wake region.[6]

PLIF Excitation and Detection

Light from a Nd:YAG laser at a wavelength of 1064 nm passes through a frequency-doubling crystal producing 532-nm light that pumps a dye laser operated with a mix of rhodamine 590 and 610 laser dyes. The dye laser outputs light at 574 nm, which is frequency-doubled and then mixed with the residual 1064-nm light to produce UV light at 226 nm. This light excites transitions in the $A^2\Sigma^+ \leftarrow X^2\Pi(0, 0)$ band of NO. Part of the beam is split off and used to monitor the laser energy and for wavelength calibration by passing it through a flame; the LIF from the flame is imaged onto a spectrometer and detected by a photomultiplier tube. Each pulse of the laser usually produces about 3 mJ of energy. A low pressure, room temperature LIF spectrum of an isolated transition determines an upper limit to the linewidth of $0.9 \pm 0.1\ \text{cm}^{-1}$. When injection-seeding the Nd:YAG laser, the laser linewidth is observed to be $0.5 \pm 0.1\ \text{cm}^{-1}$.

To determine these laser linewidths, a portion of the original beam was split off using a beamsplitter and attenuated by a neutral density filter before passing through a test cell containing a small percentage of NO in an NO/N_2 mixture at low-pressure, room temperature

conditions. The laser was then scanned in frequency over an isolated absorption line of known lineshape at these conditions. Scans were performed with low beam energies to avoid saturation effects, and the laser linewidth was used as a free parameter to produce a best fit to the experimental scan.

The larger laser linewidth of 0.9 cm^{-1} was used in the experiment to minimize pressure dependence through the overlap integral. That is, the larger laser linewidth ensured that the PLIF signal was less sensitively dependent on absorption linewidth and pressure shift.

As described, the laser frequency was selected by tuning to an absorption line in a flame. The conditions in this flame were typically at a pressure of 100 kPa and a temperature of about 1000 K. By comparison, the conditions in the mixing flowfield in the shock tunnel were typically at a pressure of 40 kPa and a temperature of about 700 K. Based on theoretical considerations,[18] there is, thus, a pressure shift of approximately 0.043 cm^{-1} in the flowfield with respect to the absorption line in the flame. This is negligible when compared with the laser linewidth and, hence, systematic errors due to this shift are considered insignificant.

The most significant error in selecting the laser frequency was due to the laser having to be tuned to a number of overlapping lines, rather than a single isolated line, in a sloping region of the spectrum. Our theoretical modeling indicated that the lowest temperature sensitivity would be achieved by tuning in a flame to a small broad peak on the wing of a larger sharper peak. The broadness of this feature, caused by the large number of overlapping lines, meant that significant uncertainity was associated with laser frequency selection. This uncertainty was worsened somewhat further by thermal drifts in laser frequency between the time of tuning and the firing of the shock tunnel. This was minimized by using the smaller laser linewidth (achieved by injection seeding) in the tuning process and completing the tuning of the laser as close as possible to the time of firing the tunnel (about a 5-min wait between tuning and firing). Tuning in a room temperature test cell was not feasible because the intensity of the small peak was too low at room temperature conditions. The experimental uncertainty in the measured fuel mole fraction resulting from the uncertainty of tuning the laser is high because we are attempting to tune to a rapidly sloping region in the spectral domain.

The UV light is formed into a sheet by expanding the laser beam in one transverse direction with a 400-mm focal length cylindrical lens and then collimating it in that direction with a 500-mm focal length spherical lens. This spherical lens also focuses the beam in the other transverse direction to a thickness of approximately 600 μm. The effect of this cylindrical-lens/spherical-lens combination is to produce a sheet of approximately constant width and slowly varying thickness. A mask before the test section decreased the width of the beam from approximately 95 to 85 mm.

The fluorescence was imaged normal to the direction of the laser sheet onto a thermoelectrically cooled ICCD camera. A UG-5 Schott glass filter was used to spectrally filter the fluorescence to remove any elastic scatter. A dye cell was used to monitor the energy variation in the laser sheet profile, which was captured on a CCD camera simultaneously with the PLIF image of the flow. This profile can be used later for correction of the image. However, we found that using this dye cell profile for correction introduced streaks into the images. More uniform images were obtained by correcting them with a region at the top of the image containing pure freestream fluid assumed to be uniform.

Results and Discussion

Figure 6a is a noninjection image for the plane-base fuel injector, which is shown by the gray mask at the left of the image. Flow is from left to right. All streamwise images have the laser sheet passing through the fuel injector nozzle centerline, parallel to the flow and perpendicular to the fuel injector strut. The laser sheet enters from the top of the image producing the shadow region beneath the fuel injectors.

Because no fuel is injected, all of the flow features are due entirely to the freestream passing over the fuel injector. The expansion around the base of the fuel injector results in a drop in pressure and

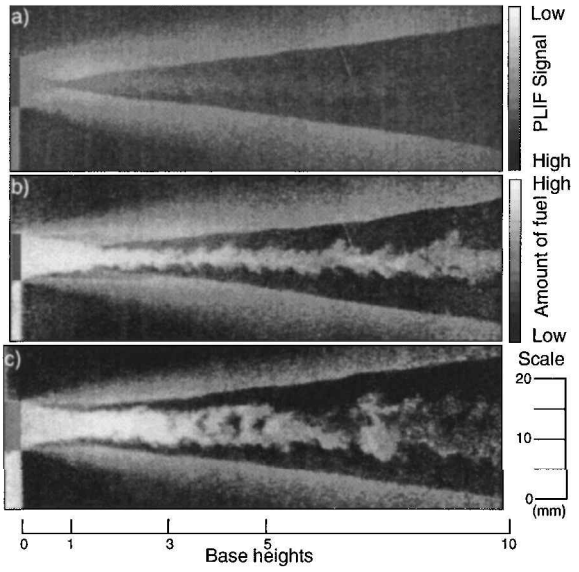

Fig. 6 Instantaneous streamwise PLIF images of the a) plane-base fuel injector with no fuel injection, b) plane-base fuel injector with fuel injection, and c) castellated fuel injector with fuel injection.

temperature and causes a decrease in PLIF signal level in this region as predicted by Fig. 2. Recompression shocks force the flow to again travel parallel to the freestream and can be seen quite clearly in the center of the image. The increase in pressure and temperature across this shock causes the signal to increase. The large variation in signal level in each of these features indicates a pressure dependence in the signal, which is greater than that expected from the analysis (see Fig. 2). We believe this is due to the assumption made when using T_{mix} in calculations. It assumes that the only variation in temperature occurs when fuel and freestream gases mix. However, temperature changes also occur across shock waves, and this is not taken into account in the analysis.

As already discussed, according to the fluid mechanical considerations, the pressure is approximately constant between the recompression shocks. The temperature is expected to vary considerably in this region. However, contrary to our original assumption, here the temperature effects are not the result of fuel and air mixing. Rather, the temperature variations are a result of variations in density through the shear layer. Nonetheless, the relatively uniform signal in this region provides evidence that our excitation method is insensitive to temperature. Outside the compression shocks, the signal level varies markedly due to the larger pressure and temperature changes. The region of validity of our PLIF model, then, is limited to the region between the recompression shocks.

The pressure dependence is larger than that expected from the analysis. This is because our modeling considers only pressure variations in the mixing flowfield, that is, in the region between the recompression shocks. Outside this region, pressure variations are accompanied by temperature variations that are unrelated to mixing. This modifies the quenching environment in a way that is different from that predicted for mixing. This means that, in the expansion fan generated at the shoulder of the injector, a quenching-dependent signal variation is observed even though the fuel mole fraction there is zero. The only way to make the signal completely independent of pressure (irrespective of location in the flow) is to further increase the quenching rate by adding more oxygen, which a good quencher, to the coflow. A consequence of adding oxygen is that the amount of NO formed during the shock reflection process is also increased. This increases the absorption, which is undesirable. Limits placed upon the tolerable amount of absorption is, thus, what has restricted the amount of quenching we could have in our experiments and is the reason why a pressure dependence remains.

Figures 6b and 6c show streamwise fuel injection images for the plane-base and castellated fuel injectors. Injection of fuel into the

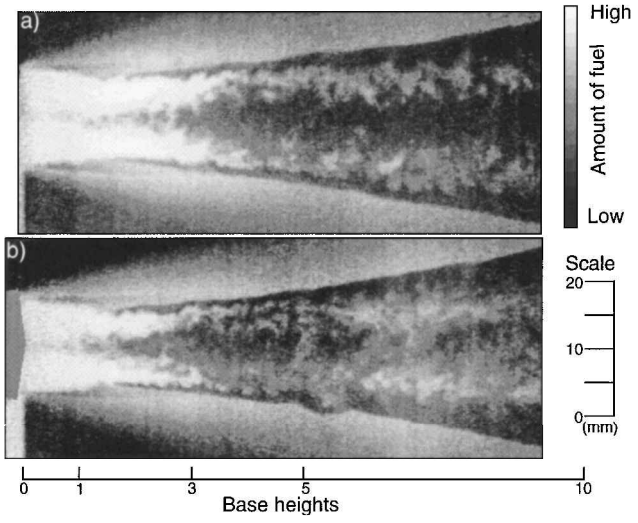

Fig. 7 Instantaneous streamwise PLIF images of fuel injectors: a) UCER and b) SCER.

flow causes the recompression shocks to be pushed farther apart. The expansions around the injector can still be seen, but they are smaller due to the change in position of the recompression shocks.

The images in Fig. 6 have not been converted to fuel mole fraction. However, the scale to the right of the fuel injection images indicates qualitatively the amount of fuel present at any point between the recompression shocks. The fuel scale is valid only between the recompression shock waves for Figs. 6b and 6c.

For both fuel injectors, the recirculation zone at the base of the fuel injectors entrains the fuel, spreading it over the entire base region. The fuel jets then narrow while passing through the wake neck before spreading out again. It is at this point that the two flowfields start to differ. The vertical spread in the fuel jet issuing from the plane-base fuel injector increases very slowly over a distance of 10 base heights. Evidence of large-scale structures inclined at about 45 deg to the flow direction are apparent.

In contrast to this, the castellated fuel injector shows a much greater vertical spread in the fuel jet over the same distance and evidence of vortex-enhanced mixing from about four base heights. After this point, there is an increasing interaction between the fuel and the freestream with the appearance of eddies, which grow with distance downstream. At about five base heights, the fuel jet appears to separate into two, most likely due to the interaction with streamwise vortices. The fuel concentration appears to decrease with downstream distance for both fuel injectors.

Both ramp fuel injectors also show entrainment of fuel near the base of the fuel injectors, as seen in Fig. 7, which shows the streamwise images for the UCER and SCER fuel injectors. After the separation of the two jets they appear to diverge. Between three and five base heights for the SCER fuel injector the fuel concentration decreases, whereas for the UCER fuel injector, the fuel concentration appears the same from near the base to the end of the imaging plane. At five base heights, the fuel concentration increases again. This feature is most likely caused by streamwise vortices generated by the injector geometry, moving the fuel in and out of the imaging plane. The fuel scale is valid only between the recompression shock waves.

The images of the streamwise planes, although highly useful, cannot provide a complete and unambiguous report of the flowfield. For instance, movement of fuel in and out of the imaged plane could be incorrectly interpreted as resulting from more rapid mixing than actually exists in the flow. When spanwise PLIF images are obtained, it is possible to remedy this shortcoming and obtain a complete picture of the flow development and the progress in the mixing process.

Because of experimental constraints that limited the optical axis to an off-axis perspective (see Fig. 4b), the spanwise images are distorted and sometimes slightly rotated. To correct for this, an image of a rectilinear grid was taken before each experiment. The distortion and rotation of the grid was then corrected using image-processing software, and the correction parameters were recorded for later use, so that an identical correction could be applied to the corresponding fluorescence image. Cross-plane images at different stages of this image correction process are shown in Fig. 8 for the plane-base fuel injector at three base-heights. Figure 8a is the original image. The result of the correction for distortion and rotation is shown in Fig. 8b. Figure 8c is the corrected image, which has been enhanced using image processing software to see the flow features clearly. The spanwise images shown in Figs. 9 and 10 have been contrast-enhanced for this purpose.

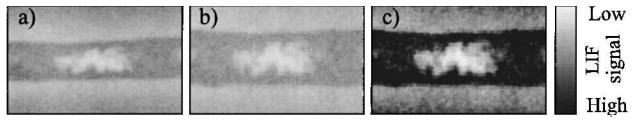

Fig. 8 Correction process shown for the plane-base fuel injector's central jet at three base heights: a) original PLIF image, b) undistorted PLIF image, and c) contrast-enhanced corrected image.

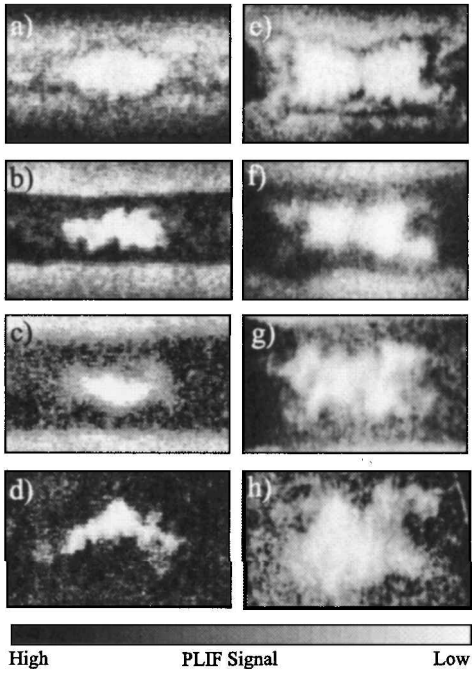

Fig. 9 Instantaneous spanwise PLIF images of plane-base and castellated fuel injectors; top to bottom 1, 3, 5, and 10 base heights. Each image is 15 mm high.

Figure 9 shows spanwise images for the plane-base (Figs. 9a–9d) and castellated (Figs. 9e–9h) fuel injectors acquired on successive tunnel runs. Flow is out of the page and the laser sheet enters the field of view from above. These images have not been converted to fuel mole fraction. The fuel jet issuing from the plane-base fuel injector does not spread much in a horizontal direction. It does contain eddylike features at the periphery of the jet, the largest of which is approximately 15% of the initial width of the jet. The interfacial length between the fuel and the freestream does not increase as rapidly as for the castellated fuel injector.

The castellated fuel injector images show fuel spreading out across the base of the fuel injector, caused by the evolution of streamwise vortices. This set of four streamwise vortices at the outer edges of the twin fuel jets are clearly visible on the left and right of Figs. 9e and 9f. These vortices appear to play a significant role in stretching the fuel–air interface at distances less than five base heights from the fuel injector but, farther downstream, they dissipate leaving eddies to assume the dominant role in further fuel–air mixing. These eddies in the castellated fuel injector flowfield are of similar size to those in the plane-base fuel injector flowfield, and are present in similar numbers.

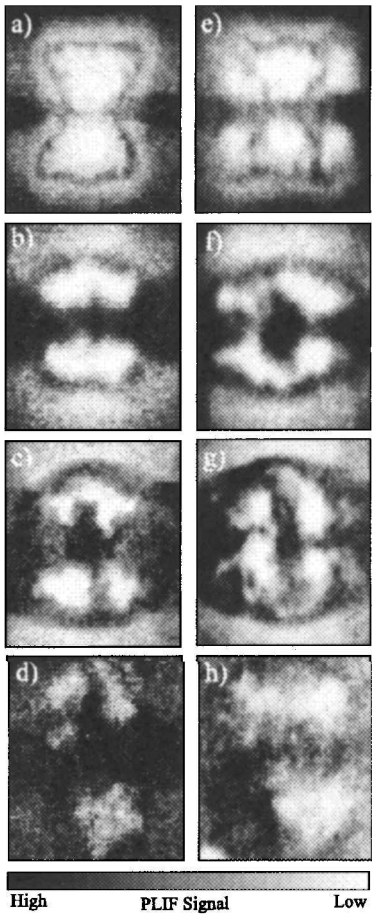

Fig. 10 Instantaneous spanwise PLIF images of UCER and SCER fuel injectors; top to bottom 1, 3, 5, and 10 base heights. Each image is 30 mm high.

Figure 10 shows the spanwise images for the UCER (Figs. 10a–10d) and SCER (Figs. 10e–10h) fuel injectors. At one base height, the UCER fuel injector shows a greater fuel spread across the base of the fuel injector. In both flows, the two fuel jets are quickly separated into four regions. This is thought to be due to powerful streamwise vortices originating in the flow at the vertical downstream edges of the ramps. The vortices are still apparent at five base heights. This indicates that the vortices produced by the ramp fuel injectors are stronger than those produced by the castellated fuel injector, which, by five base heights, have dissipated. In addition to this, the mixing for the ramp fuel injectors is seen to be more efficient than the castellated fuel injector. Unlike the vortices produced by the castellated fuel injector, which affect only the periphery of the fuel-rich region, the UCER and SCER vortices appear to cause large intrusions of fuel-lean fluid into the center of the fuel-rich region from either side. These intrusions cause the increase in the interfacial area by separating the fuel-rich regions into four distinct areas. By the time the flow reaches 10 base heights downstream, the vortices appear to have dissipated.

When comparing the UCER fuel injector to the SCER fuel injector, it appears that the SCER fuel injector is slightly more effective at enhancing mixing. At each downstream position, the vortices produced by the UCER fuel injector are not as strong as those produced by the SCER fuel injector. The degree of mixing in the flow produced by the SCER injector appears to be slightly more advanced than that of the UCER injector at each position. Similarly, the interfacial area between fuel and freestream for the UCER fuel injector is not as great as that for the SCER fuel injector. In apparent contradiction of this inference, the fuel in Fig. 10d seems more dilute than in 10h, indicating that the UCER fuel injector has a better mixing performance at 10 base heights.

The image of Fig. 8b is shown converted to fuel mole fraction in Fig. 11 for both an instantaneous and an averaged PLIF image.

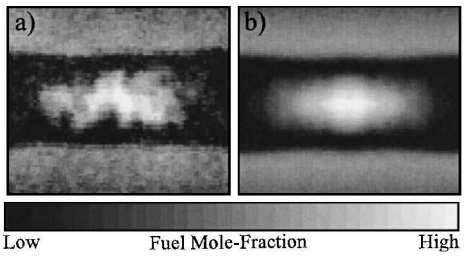

Fig. 11 Fuel mole-fraction images for the plane-base fuel injector's central jet at three base heights: a) instantaneous result and b) averaged result.

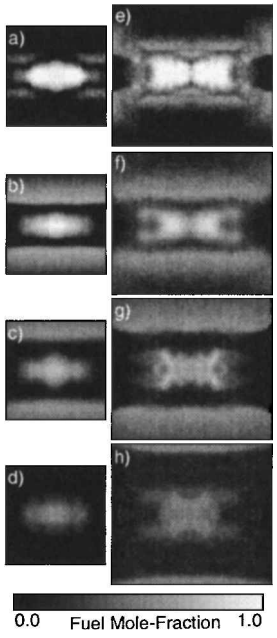

Fig. 12 Averaged PLIF images converted to mole fraction for plane-base and castellated fuel injectors; top to bottom 1, 3, 5, 10 base heights. Images on left are 15 mm high. Images on right are 30 mm high.

These images have been converted using theoretical relations between PLIF signal level and mole fraction such as those shown in Fig. 2. Again, fuel scale is valid only between the recompression shocks. By the use of computational fluid dynamics (CFD) calculations, the pressure is predicted for each fuel injector flowfield at each position downstream. This is then the pressure used to determine the theoretical relation between PLIF signal level and fuel mole fraction and convert the images. Were we able to completely remove the pressure dependence, the use of CFD data in this way would be unnecessary. This is one motivation for further work to reduce the pressure sensitivity even further.

The corrected instantaneous image shown in Fig. 11a is useful for comparison with time-dependent CFD calculations. However, to allow for future comparisons with time-averaged CFD calculations, the images are averaged by invoking symmetry and, for the plane-base fuel injector, also by averaging the results from each of the three nozzles on each fuel injector configuration such as the image seen in Fig. 11b. This averaging process relies on the assumption that the time-averaged flow associated with neighboring nozzles for a particular fuel injector are identical. It was used in the current work in preference to averaging over a large number of experimental runs because of time constraints on the facility. Only the plane-base and castellated fuel injectors will be subjected to this analysis because the contribution of pressure variations to the PLIF signal for the ramp fuel injectors is too great to allow meaningful results to be obtained at present.

Figure 12 shows the averaged images converted to mole fraction. Note that the conversion to mole fraction via our theoretical modeling is only valid between the recompression shocks, where the pressure is relatively constant. This limitation must be taken into

account when viewing Fig. 12. Figures 12a–12d show the plane-base fuel injectors and Figs. 12e and 12h the castellated fuel injectors.

Uncertainty Analysis

To determine how accurately the fuel mole-fraction can be measured using this model, we have calculated the sensitivity to the uncertainty in the most important fluid mechanical and spectroscopic parameters. A normalized sensitivity parameter ϵ_i is defined in terms of a generalized fluid mechanical or spectroscopic parameter ζ_i as

$$\epsilon_i \approx \frac{\delta S_i/S}{\delta\zeta_i/\zeta_i} \tag{8}$$

The sensitivity ϵ_i gives a value that relates the uncertainty in the PLIF signal, S, to a given uncertainty in the parameter, ζ_i. A value of unity for ϵ_i, for example, indicates that a 1% uncertainty in the parameter produces a 1% uncertainty in the signal level.

In our work, we have sought to design our experiment such that the fuel mole fraction can be determined as a simple function of the fluorescence signal. Designating the fuel mole-fraction χ_{fuel} as the first generalized parameter ζ_1, we have sought to achieve the functional dependence

$$\chi_{\text{fuel}} = \zeta_1 = \zeta_1(S) \tag{9}$$

However, although we have achieved strong sensitivity of S to χ_{fuel}, the signal still has a weak dependence on other parameters. That is,

$$\chi_{\text{fuel}} = \zeta_1 = \zeta_1(S, \zeta_2, \ldots, \zeta_i, \ldots) \tag{10}$$

Hence, correction for the effects of these other parameters need to be considered. Uncertaintities in the values of these parameters will contribute to the overall uncertainty of determining the fuel mole fraction. These considerations lead to the following estimate of the relative uncertainty in the fuel mole fraction:

$$\frac{\delta\chi_{\text{fuel}}}{\chi_{\text{fuel}}} = \frac{\delta\zeta_1}{\zeta_1} = \frac{1}{\epsilon_1}\sqrt{\left(\frac{\delta S}{S}\right)^2 + \sum_{i\neq 1}\left(\frac{\delta S_i}{S}\right)^2}$$

$$= \frac{1}{\epsilon_1}\sqrt{\left(\frac{\delta S}{S}\right)^2 + \sum_{i\neq 1}\left(\epsilon_i\frac{\delta\zeta_i}{\zeta_i}\right)^2} \tag{11}$$

This analysis can be used to estimate the uncertainty in the fuel mole fraction determined from the analysis of the PLIF images. We have used our modeling of the fluorescence to convert the PLIF images to images of fuel mole fraction. This conversion works reasonably well for the region between the recompression shocks, but is unreliable outside that region. To estimate the uncertainty in determining χ_{fuel} in the region between the recompression shocks, we have determined the values of the sensitivities ϵ_i for the most important independent parameters for conditions where $\chi_{\text{fuel}} = 0.5$, $P = 40$ kPa, and $T = 445$ K. These values are listed in Table 1. Because of the approximately linear relationship between S and χ_{fuel} in the region between the recompression shocks, the value of ϵ_1 in that region is very close to 1.0.

As seen from this table, at these conditions, the PLIF signal level is most sensitive to the amount of O_2 present initially in the shock tube. For this parameter, the PLIF signal level decreases by 2.2% for every 1.0% increase in the amount of O_2. The sensitivity of the PLIF signal to the amount of oxygen is mainly caused by the effect it has on the quench rate in the freestream. Oxygen has quite a high quenching cross section, so that an increase in the amount of oxygen present in the flow increases the quench rate and correspondingly the PLIF signal level decreases.

Changes in temperature, pressure, and laser linewidth all produce relatively smaller changes in the PLIF signal level. The PLIF signal changes by about only 0.06% for a 1% change in temperature, indicating that our modeling has reduced the temperature dependence considerably. The PLIF signal level varies by only 0.15% for a 1% change in pressure at these conditions. Only a 0.24% change in signal level occurs when there is a 1% change in laser linewidth $\Delta\nu_l$. This is as expected because we are using a broad laser and overlapping a number of transitions. Therefore, a small change in linewidth should not have much effect on the signal produced. However, small changes in laser frequency produces a significant change in PLIF signal level. Hence, the change in laser frequency was calculated as a percentage change compared to the laser linewidth, resulting in a near-unity sensitivity. The uncertainty in the measured signal level is largely due to detector shot noise, which produces a relative uncertainty $\delta S/S$ of about $\pm 4.0\%$.

Table 1 Sensitivities ϵ_i and fractional uncertainties $\delta\zeta_i/\zeta_i$ contributing to uncertainty in determining fuel mole-fraction from measured PLIF singnal[a]

Parameter	ϵ_i	$\delta\zeta_i/\zeta_i$	$\epsilon_i(\delta\zeta_i/\zeta_i)$
T	0.062	0.10	0.006
p	0.15	0.10	0.02
ν_l	0.95	0.15	0.14
$\Delta\nu_l$	0.24	0.11	0.03
$\chi_{O_2}^{\text{freestream}}$	−2.2	0.02	−0.05
S	1.0	0.04	0.04

[a]Fractional uncertainty in determining the fuel mole-fraction from the measured fluorescence signal can be estimated by adding the uncertainties given in the right column in quadrature, as stipulated by Eq. (11), where $\epsilon_i = 1$.

Combining the uncertainties in the experimental and theoretical parameters through Eq. (11) shows that a fractional uncertainty for measuring the fuel mole fraction at a value of 0.5 is $\pm 15.8\%$. That is, for $\chi_{\text{fuel}} = 0.5$, the absolute uncertainty is ± 0.08. Similar uncertainty analyses for other fuel mole fractions show that the fractional uncertainty varies monatonically from $\pm 15.0\%$ near $\chi_{\text{fuel}} = 0$ to $\pm 18.5\%$ near $\chi_{\text{fuel}} = 1$.

Based on this uncertainty determination, this mole-fraction-sensitive imaging method can now be used with some confidence in measuring fuel mole fractions, with the caution that it can only be used in areas of relatively constant pressure. The sensitivity analysis has shown which parameters must be known accurately; one of the most important is the amount of O_2 in the shock tube. The most dominant source of error, however, was the ability to tune the laser to the chosen transition frequency. An improvement in the method used for tuning the laser accurately to a sloping part of the absorption spectrum is, thus, expected to lead to an improved accuracy with which χ_{fuel} can be determined in regions of low to moderate pressure variations. Finding a method whereby the collisional quenching can be significantly increased without significantly increasing absorption will allow the method to be used successfully for flows with much larger pressure gradients.

Conclusions

A theory for instantaneous PLIF imaging of fuel mole fraction in a flow with pressure gradients and large temperature variations has been presented. The aim was to achieve PLIF signal level proportional to fuel mole fraction, independent of temperature and pressure.

The PLIF signal was strongly dependent on the gas composition, laser excitation frequency, and linewidth. We chose gases with sufficiently high quenching cross section to achieve $Q \approx 10A$, reducing the signal's pressure dependence. However, this amount of quenching needs to be increased to further decrease the pressure dependence. The laser excitation frequency and linewidth were chosen to overlap a number of transitions with both low- and high-J rotational numbers. This assisted in removing the temperature dependence of the signal. Optimizing the parameters in the PLIF signal equation allowed us to produce a signal proportionality to fuel mole fraction in regions of the flow dominated by mixing.

Experimental PLIF images in the mixing regions of plane-base, castellated, UCER, and SCER fuel injectors were obtained in both streamwise and spanwise planes using the optimum laser frequency and other conditions specified by the theory. The streamwise images

showed evidence of large-scale structures and show that the signal is proportional to fuel mole fraction and insensitive to temperature. However, the images did show pressure dependence with the expansion around the fuel injectors and the recompression shocks being clearly visible in the streamwise images. This pressure dependence was smaller for the plane-base and castellated fuel injectors than for the ramp fuel injectors, making the images of the former amenable to further analysis and conversion to fuel mole-fraction images.

Analysis of the spanwise images for the plane-base and castellated injectors allowed qualitative comparisons to be made of their relative mixing efficiencies.

References

[1]Gutmark, E. J., Schadow, K. C., and Yu, K. H., "Mixing Enhancement in a Supersonic Free Shear Flow," *Annual Review of Fluid Mechanics*, Vol. 27, Jan. 1995, pp. 375–417.

[2]Gaston, M. J., Mudford, N. R., and Houwing, A. F. P., "A Comparison of Two Hypermixing Fuel Injectors in a Supersonic Combustor," AIAA Paper 98-0964, Jan. 1998.

[3]Tarnopolsky, A., and Gai, S. L., "Investigation into the Mixing Layer due to Two Parallel Mixing Streams," *Proceedings of the 20th Congress of the International Council of the Aeronautical Sciences*, Sept. 1996.

[4]Fox, J. S., Danehy, P. M., and Houwing, A. F. P., "Instantaneous PLIF Measurement of Species Mole-Fraction in a Varying Temperature Supersonic Flow," *Proceedings of the 21st Congress of the International Council of the Aeronautical Sciences*, 1998.

[5]McIntyre, T. J., Houwing, A. F. P., Palma, P. C., Rabbath, P. A. B., and Fox, J. S., "Optical and Pressure Measurements in Shock Tunnel Testing of a Model Scramjet Combustor," *Journal of Propulsion and Power*, Vol. 13, No. 3, 1997, pp. 388–394.

[6]Gai, S. L., Tarnopolsky, A., O'Byrne, S., Houwing, A. F. P., and Mudford, N. R., "Constrained and Unconstrained Compressible Mixing Layers," *Proceedings of the 21st International Symposium on Shock Waves*, July 1997.

[7]Stalker, R. J., Morgan, R. G., and Netterfield, M. P., "Wave Processes in Scramjet Thrust Generation," *Combustion and Flame*, Vol. 71, Jan. 1988, pp. 63–77.

[8]McMillin, B. K., Palmer, J. L., and Hanson, R. K., "Temporally Resolved, Two-Line Fluorescence Imaging of NO Temperature in a Transverse Jet in Supersonic Cross Flow," *Applied Optics*, Vol. 32, No. 36, 1994, pp. 7532–7545.

[9]Hiller, B., and Hanson, R. K., "Simultaneous Planar Measurements of Velocity and Pressure Fields in Gas Flows Using Laser-Induced Fluorescence," *Applied Optics*, Vol. 27, No. 1, 1999, pp. 33–48.

[10]Palmer, J. L., McMillin, B. K., and Hanson, R. K., "Planar Laser-Induced Fluorescence Imaging of Velocity and Temperature in Shock Tunnel FreeJet Flow," AIAA Paper 92-0762, 1992.

[11]Lozano, A., Smith, S. H., Mungal, M. G., and Hanson, R. K., "Concentration Measurements in a Transverse Jet by Planar Laser-Induced Fluorescence of Acetone," *AIAA Journal*, Vol. 32, No. 1, 1994, pp. 218–221.

[12]Hartfield, R. J., Hollo, S. D., and McDaniel, J. C., "Planar Measurement Technique for Compressible Flows Using Laser-Induced Iodine Fluorescence," *AIAA Journal*, Vol. 31, No. 3, 1993, pp. 483–490.

[13]Allen, M. G., Parker, T. E., Reinecke, W. G., Legner, H. H., Foutter, R. R., Rawlins, W. T., and Davis, S. J., "Fluorescence Imaging of OH and NO in a Model Supersonic Combustor," *AIAA Journal*, Vol. 31, No. 3, 1993, pp. 502–512.

[14]Ruyten, W. M., Williams, W. D., and Heltsley, F. L., "Computational Flow Imaging for Planar Laser-Induced Fluorescence Applications (CFI-PLIF," AIAA Paper 94-2621, June 1994.

[15]Paul, P. H., Gray, J. A., Durant, J. L., and Thoman, J. W., "Collisional Quenching Corrections for Laser-Induced Fluorescence Measurements of NO $A^2\Sigma^+$," *AIAA Journal*, Vol. 32, No. 8, 1994, pp. 218–221.

[16]Vincenti, W. G., and Kruger, C. H., *Introduction to Physical Gas Dynamics*, Wiley, New York, 1965, pp. 132–134, Chap. 4.

[17]Gross, K. P., McKenzie, R. L., and Logan, P., "Measurements of Temperature, Density, Pressure, and Their Fluctuations in Supersonic Turbulence Using Laser-Induced Fluorescence," *Experiments in Fluids*, Vol. 5, No. 6, 1987, pp. 372–380.

[18]DiRosa, M. D., "High-Resolution Line Shape Spectroscopy of Transitions in the Gamma Bands of Nitric Oxide," Ph.D. Dissertation, Dept. of Mechanical Engineering, Stanford Univ., Stanford, CA, 1996.

[19]Clemens, N. T., "An Experimental Investigation of Scalar Mixing in Supersonic Turbulent Shear Layers," Ph.D. Dissertation, Dept. of Mechanical Engineering, Stanford Univ., Stanford, CA, 1991.

[20]McMillin, B. K., "Instantaneous Two-Line PLIF Temperature Imaging of Nitric Oxide in Supersonic Mixing and Combustion Flow Fields," Ph.D. Dissertation, Dept. of Mechanical Engineering, Stanford Univ., Stanford, CA, 1993.

[21]Vardavas, I. M., "Modelling Reactive Gas Flows Within Shock Tunnels," *Australian Journal of Physics*, Vol. 37, No. 2, 1984, pp. 157–177.

[22]Magi, E. C., and Gai, S. L., "Flow Behind Castellated Blunt-Trailing-Edge Aerofoils at Supersonic Speeds," *Journal Fluid Mechanics*, Vol. 375, Nov. 1998, pp. 85–111.

[23]Stalker, R. J., "The Free-Piston Shock Tunnel," *AIAA Journal*, Vol. 5, No. 12, 1967, pp. 34–38.